Superlattices and Microstructures, Vol. 21, No. 4, 1997

State-filling and magneto-photoluminescence of excited states in InGaAs/GaAs self-assembled quantum dots

S. Raymond†, S. Fafard, P. J. Poole, A. Wojs‡,
P. Hawrylak, C. Gould§, A. Sachrajda, S. Charbonneau
Institute for Microstructural Sciences, National Research Council,
Ottawa, Ontario, Canada, K1A 0R6

D. Leonard¶, R. Leon‖, P. M. Petroff, J. L. Merz∗∗
Center for Quantized Electronic Structures (QUEST) and Materials Department
and Electrical and Computer Engineering Department,
University of California, Santa Barbara, California 93106, U.S.A.

(Received 15 July 1996)

We present the first radiative lifetime measurements and magneto-photoluminescence results of excited states in InGaAs/GaAs semiconductor self-assembled quantum dots. By increasing the photo-excitation intensity, excited state interband transitions up to $n = 5$ can be observed in the emission spectrum. The dynamics of the interband transitions and the inter-sublevel relaxation in these zero-dimensional energy levels lead to state-filling of the lower-energy states, allowing the quasi-Fermi level to be raised by more than 200 meV due to the combined large inter-sublevel spacing and the low density of states. The decay time of each energy level obtained under various excitation conditions is used to evaluate the inter-sublevel thermalization time. Finally, the emission spectrum of the dots filled with an average of about eight excitons is measured in magnetic fields up to 13 Tesla. The dependences of the spectrum as a function of carrier density and magnetic field are compared to calculations and interpreted in terms of coherent many-exciton states and their destruction by the magnetic field.

Key words: quantum dots, optical properties, carrier relaxation.

† Also at Department of Physics, University of Ottawa, Ottawa, Ontario, Canada, K1N 6N5.

‡ Also at Department of Physics, Technical University of Wroclaw, Wroclaw 50-370, Poland.

§ Also at CRPS, University of Sherbrooke, Sherbrooke, Quebec, Canada, J1K 2R1.

¶ Present address: Santa Barbara Research Center, Santa Barbara, California, U.S.A. 93117.

‖ Present address: Department of Electronic Materials Engineering, The Australian National University, Canberra, ACT, 0200, Australia.

∗∗ Present address: Department of Electrical Engineering, University of Notre Dame, Notre Dame, Indiana U.S.A. 46556-5602.

0749–6036/97/040541 + 18 $25.00/0 sm960194

1. Introduction

Nanostructures, involving quantum confinement in more than one dimension, have become the focus of scientific interest and research because of their potential in uncovering new phenomena in solid state physics and their potential in device applications [1, 2]. In order for one-dimensional and zero-dimensional heterostructures to be of any use in optoelectronic applications, however, a number of criteria in their structural qualities need to be met. Formation of distinct zero-dimensional (0D) sublevels in the energy spectrum require that the potential wells defining the dots be sufficiently narrow and uniform to yield subband separation larger than the available thermal energy ($\Delta E > k_B T$), and that the subband energy fluctuations be smaller than the subband separation ($\delta E < \Delta E$). Furthermore, the quasi-Fermi level E_F should be sufficiently low to avoid the population of excited quantum dot (QD) states. There are additional constraints imposed on QDs for optoelectronic applications. First, the QD interfaces should be free of defects in order to minimize nonradiative recombination effects which reduce quantum efficiency and carrier lifetime. To achieve this objective, fabrication techniques in which the dots are formed completely *in situ* during epitaxial growth seem very attractive. Second, in order to ensure adequate interaction between the confined carriers and an optical beam, high density and uniform arrays of dots are desirable. Finally, an efficient mechanism of carrier capture from the surrounding barriers into the QD is essential to utilize efficiently optically or electrically injected carriers in the devices.

Various fabrication techniques of QDs have been proposed based on high resolution patterning with or without subsequent regrowth [3], namely, disordering induced by a laser [4] or ion beam [5], and lateral strain modulation with stressors [6, 7]. However, these approaches require complex nanofabrication processes. In addition, process-induced inhomogeneities and adjacent regrown interfaces may severely affect the optical properties of the dots [8].

One of the promising recent advances in the fabrication of these devices which avoids most of these technological problems exploits one of the natural consequences of the sequential growth of dissimilar materials [9–11]. This, together with the relative simplicity and intrinsic quality, is one of the main reasons for the recent success of the so-called self-assembled growth techniques to produce quantum dots [12–14]. Such a growth technique has been used for the production of III–V semiconductor quantum dots which were shown to exhibit both a separation between quantum confined levels larger than room temperature thermal energy and an inhomogeneous broadening of these levels much smaller than the same quantity. As mentioned previously, these prerequisites are mandatory for the realization of active quantum dot lasers.

When the deposited thickness exceeds the critical value, the epitaxy of a highly lattice mismatched ($\sim 4\%$) semiconductor onto a substrate results in the formation of three-dimensional islands, several monolayers high with quantum lateral dimensions. When the island formation follows the Stranski–Krastanov [9–11] growth mode, they lie upon a one or few monolayers thick of the deposited material, referred to as the wetting layer (WL). This transition to a 3D growth mode has been observed for a number of III–V material systems based on Ga, Al, In, and As, P, and Sb, and also with Ge/Si [9]. QDs are obtained when these islands are overgrown with a barrier material. The spontaneous island formation during growth precludes the interface quality problems often associated with *ex situ* processed quantum structures of low dimensionality. This breakthrough in the fabrication of defect-free 0D structures provides the opportunity for experimental verification of the effect of three dimensional quantum confinement in semiconductor structures and in their potential for use in device application.

One of the fundamental remaining questions with regards to the confinement of carriers in three dimensions involves the study of carrier relaxation (thermalization) and carrier capture in QD structures. Apart from the basic scientific interest of this issue, its understanding is an important requirement for the improvement of many optoelectronic devices such as light emitting diodes or lasers. The dynamics of carriers confined in semiconductor quantum structures with allowed momentum in at least one direction leads to rapid thermal-

ization with the lattice, and consequently radiative recombination originating predominantly from the lowest available state(s).

For QDs however, the 0D discrete density-of-states imposes more severe thermalization rules [15, 16] which can translate to the observation of photoluminescence (PL) from excited state transitions at low excitation intensities due to the restricted inter-sublevel relaxation rates [4]. Due to this phonon bottleneck effect, efficient carrier relaxation towards the ground states occur predominantly between levels which are separated by not more than a few meV using longitudinal acoustic (LA) phonon emission, or by an energy within a few meV from the longitudinal optic (LO) phonon energies [17–19]. However, it has been shown that thermalization can also be achieved efficiently due to multi-phonon processes [18, 20] or Coulomb interactions [21]. For example, the inhomogeneously broadened Gaussian PL lineshape originating from the statistically distributed ground states of small self-assembled QDs obtained using the spontaneous island formation [22–28] indicates that the inter-sublevel relaxation rates are much faster than the $\sim$ 1 ns interband dynamics of the ground states [29]. Furthermore, the atomic-like discrete energy spectrum of each QD state is expected to lead to a state-filling effect due to exclusion principles taking effect when only a few carriers populate the lower states. This will also lead to suppressed inter-sublevel dynamics and to the observation of excited state interband transitions as the excitation intensity is increased. This has also been observed experimentally with larger self-assembled QDs [17, 30] which support a greater number of excited states [31], with hole levels in small pyramidal self-assembled QDs [32], and with QDs created by potential deformation in a quantum well (QW) stressed with self-assembled QDs [33]. The phonon bottleneck and the state filling effects lead to emission peaks at higher energy than the ground state emission, but should not be confused with the higher energy emission commonly observed in the case of monolayer (ML) fluctuations in a QW. Indeed the excitons localized in the potential fluctuation of a QW can be used to produce natural QDs [34–36]. Micro-PL spectroscopy of these natural QDs revealed the very sharp homogeneous linewidth of the ground state emission similar to the one observed with self -assembled QDs [23, 24, 20], and excitation spectroscopy has also been used to reveal the excited states which have a energy splitting comparable to the QW inhomogeneous broadening. In the absence of the strain-induced self-assembling processes [37, 38], monolayer fluctuations can lead to segregated inhomogeneous broadening resulting in multi-peak PL emission when observed in macro-spectroscopy. For example Marquezini *et al*. recently reported PL emission of thin InAs/InP QWs displaying up to five peaks corresponding to the ground state PL emission in QWs having a local thickness of 1 to 5 MLs respectively [39].

The above three effects (phonon bottleneck, state-filling, and segregated inhomogeneous broadening) can give rise to higher energy emission peak(s), but each possesses characteristic features specific to the different physics involved in each effect. For example, the state filling effect is the only one which will show clear saturation effects. At low intensities only the (inhomogeneously broadened) ground state levels are observed because of the fast inter-sublevel relaxation in the case of bare levels with no significant phonon bottleneck effect. As the intensity is increased, a progressive saturation of the lower energy transitions is combined with the emergence of new emission peaks originating from the excited state interband radiative transitions. These are observed as the inter-sublevel carrier relaxation towards the lower level is slowed due to the reduced number of available final states [17, 30, 32, 33]. In contrast the phonon bottleneck effect will permit excited state interband transitions even in low excitation conditions because the inter-sublevel and interband relaxation dynamics are comparable [4]. On the other hand, the multiple peaks observed in the case of segregated inhomogeneous broadening are usually observed with the same relative amplitude over several orders of magnitude of excitation intensity since they reflect the relative abundance of a given ground state energy relative to the other available ground state energies in the probed area [39]. Consequently, the energy position of the peaks observed in the case of segregated inhomogeneous broadening in QWs follow the energy predicted for a QW with a fluctuation of a few MLs from its mean deposited thickness. In contrast, in self-assembled QDs the energy spectra of the excited states are typically quite different from the ML fluctuation energies due to the lateral confinement. Also, in contrast to the other two cases, the higher energy peaks observed in the case of the segregated inhomogeneous broadening all originate from ground state transitions which will behave

very differently under an external perturbation. For example, in a magnetic field the ground states will exhibit normal diamagnetic shifts whereas the excited states will show more complex splitting with shifts to lower energies and with restoration of the dynamical symmetry at some specific fields [31, 40–42]. The excitons localized in natural dots in thin QWs with ML fluctuations are confined by a much shallower potential than for self-assembled QDs and are therefore easily distinguished when the available thermal energy is increased [43, 44]. The onset of thermionic emission and the thermal PL quenching is therefore observed at much higher temperatures in self-assembled QDs due to their deeper confining potentials.

By virtue of their relatively rapid inter-sublevel dynamics and well defined 0D density of states, larger self-assembled QDs, which can accommodate several excited states with an electronic inter-sublevel spacing comparable to the LO phonon energy, represent an ideal quantum system to study state filling effects. For example, the observed PL peak separation between the radiative recombination of adjacent excited states in self-assembled QDs 36.5 nm in diameter is $\sim$ 50 meV [17]. This allows the excited state transitions to be resolved from the Gaussian inhomogeneous broadening which for self-assembled QDs typically yields a full-width-half-maximum (FWHM) of $\sim$ 50 meV. This broadening arises from small fluctuations in QDs confining-size, the alloy compositions variations, and the shifts due to strain-field effects. The major contribution to the inhomogeneous broadening comes from the size variation due to the large confining potentials and the small volumes. However, due to the self organizing processes, segregated inhomogeneous size broadening is not normally observed in InGaAs/GaAs self-assembled QDs (i.e. only one size of islands and its associated normal distribution). Under favorable growth conditions, the alloy fluctuations can be minimized and would certainly never lead to segregated inhomogeneous alloy broadening under normal conditions. Finally, although the total energy shifts due to strain fields are more than a hundred meV [45, 46], the QD to QD variations are again small due to the self-organization of the strain fields leading to a normal distribution of the next-neighbor distances [47, 48] which also prevent the possibility of segregated inhomogeneous strain-field broadening. In addition, many-body phenomena such as biexcitons, charge-excitons, exciton-complexes, and bandgap renormalization can also contribute to the broadening at higher excitation intensities, but for a large ensemble of QDs they will be difficult to resolve from the above inhomogeneous broadening mechanisms as they can only shift the emission energy by few meV [31, 46].

It is the purpose of this paper to analyse the dynamics of excited states in such self-assembled QDs with well defined excited states spectra, and for the first time study the influence of the state filling on the inter-sublevel thermalization and the interband radiative recombination. We also present the results from measurements and calculations of the effect of carrier density and of magnetic field on the recombination processes in these self-assembled QDs. The magnetic field experiments allow us to unambiguously identify the nature of the recombination spectrum in terms of excited states of many exciton complexes in QDs.

2. Sample

The self-assembled QDs used for the present study exhibit state-filling with up to four observable excited state interband transitions [17]. The sample has been grown by molecular beam epitaxy (MBE) using the Stranski–Krastanow growth mode. The sample structure grown on a GaAs (100) substrate, consists of a 500 nm GaAs buffer layer, followed by the QD layer where 6.5 MLs of $In_{0.5}Ga_{0.5}As$ were grown at a nominal temperature of 530 $^{\circ}$C, and covered with a 30 nm GaAs cap layer. The PL measurements were performed at 4 K using for the excitation source either a steady state (CW) Ar^{+}, or a YAG pumped rhodamyne 640 dye laser system providing 5 ps pulses at 630.0 nm at a repetition rate of 76 MHz. The beam was focused to a spot $\sim 80\ \mu$m in diameter at the sample surface, thus probing a population of $\sim 5 \times 10^5$ dots. The luminescence was dispersed by a 0.64 m spectrometer and either detected with a cooled germanium detector using synchronous detection techniques for the CW measurements, or collected and analysed via an up-conversion technique using a $LiIO_3$ crystal for the time-resolved PL (TRPL) measurements [47]. This TRPL system provided a temporal resolution of $\sim$ 10 ps.

The magneto-PL measurements were performed at $T \approx 4$ K using the same excitation source. The excitation beam was passed through a 35 m long multi-mode fiber with a core diameter of 100 μm which had its end placed directly above the sample surface inside the coil-magnet. The luminescence signal was passed through the same fiber and then dispersed with a 0.64 m spectrometer and detected with a resolution of 0.4 nm using a cooled germanium detector with standard synchronous detection techniques. The transmission spectra of the fiber was verified independently and used to correct the PL spectra for the fiber absorption. From the pumping power, cross-section of the fiber, and the time-resolved experiments to be presented below, we estimate to have an average number of $N = 2$–10 excitons per dot, corresponding to the areal density of 0.2–1.0×10^{12} cm^{-2}.

Transmission electron microscopy (TEM) was performed on a piece adjacent [48] to the sample studied optically to ensure that the self-assembling growth proceeded normally, and that no segregated inhomogeneous size or strain-field broadening can be present in the PL spectra due to monolayer fluctuations or gross size or distribution non-uniformities. As can be inferred from Fig. 1, the dot density is 100 μm^{-2} and their average diameter is 36.5 nm, which yields a coverage of 10%. Note that the inset shows that the QD size uniformity is better than 10%.

3. Steady state photoluminescene

Figure 2A and B show the CW PL spectra obtained for different excitation intensities. At very low excitation density (0.050 W cm^{-2}), only one emission peak is observed at 1.10 eV with a shoulder at 1.13 eV. As the power is increased, five peaks are resolved including the ground state [17]. These peaks are separated by $\sim$ 40 meV (in the case of the highest excited states) and $\sim$ 50 meV (in the case of the lowest states). Their FWHM ranges from 30 to 40 meV, as deduced from a multiple Gaussian fit. Figure 2C shows the time-integrated spectra obtained for pulsed excitation. Also, for comparison, the calculated emission energies for a corresponding hypothetical QW with various numbers of MLs are shown at the top of Fig. 2. From the good QD size and near-neighbor distance uniformities observed in Fig. 1 and from the complete lack of correlation of the emission energies with the emission expected for ML fluctuations, the possibility of segregated inhomogeneous broadening can be unambiguously ruled out†. Furthermore, the emission peaks observed in Fig. 2 have the temperature dependence expected for excitons localized in deep confining potentials [44]. For this sample, some radiative recombination can still be observed at room temperature, whereas excitons localized in shallow minima suffering from segregated inhomogeneous broadening would be quenched at much lower temperatures depending on the localization potential (typically a few tens of Kelvins [43]). The excited-state nature of these higher energy transitions will be clearly revealed in Section 5 by measuring the magnetic field dependence of these high energy satellites [42].

The detailed temperature dependence of the PL emission spectrum, in the high optical excitation regime (where excited states can be observed), was obtained and this dependence is shown in Fig. 3. It is clear, from the figure, that as the temperature is increased, the number of high energy satellites is reduced. This quenching effect starts with the highest excited state peak and progressively moves towards the lower lying peaks as the temperature is increased, such that at $T = 225$ K, only the low energy $n = 1$ transition can be observed. It should also be emphasized that a PL signal was detected up to room temperature with a modest excitation power density of 50 W cm^{-2}. This is a clear indication that this growth technique is capable of producing QDs of very high optical quality with very few nonradiative recombination sites present. The red shift observed as the temperature is increased reflects the reduction of the bandgap with temperature.

The quenching effect observed at high temperatures can be understood simply by the thermionic emission of the photocarriers out of the QD into the wetting layer material. As will be derived in the next section, the energy difference between the various levels and the wetting layer continuum ('activation energy') are:

† The possibility of segregated inhomogeneous alloy broadening remains, but it has never been observed and is therefore highly unlikely especially since it would not lead to intensity-dependent features.

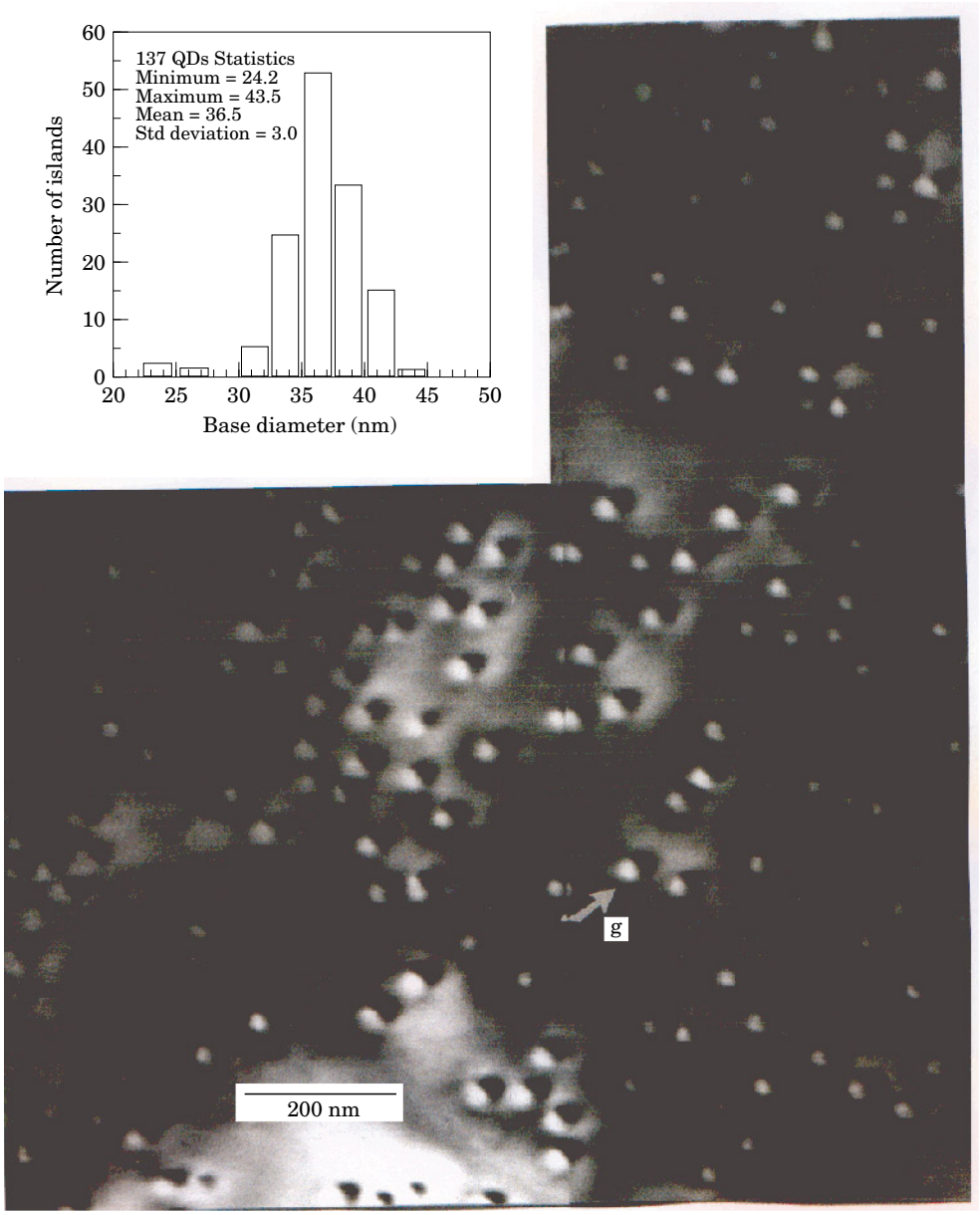

Fig. 1. Dark field TEM plan view micrograph of the InGaAs/GaAs sample. The dark/light contrast seen is obtained under two beam dynamical diffraction conditions. The operating diffraction vector is always perpendicular to the dark/light lobes, indicating a radially symmetric strain field. The inset shows some statistics obtained from the TEM picture.

$\Delta E_{1-wl} \sim 160$ meV, $\Delta E_{2-wl} \sim 130$ meV and, $\Delta E_{3-wl} \sim 100$ meV. Therefore, a deeper confinement clearly leads to thermal quenching at higher temperature [44].

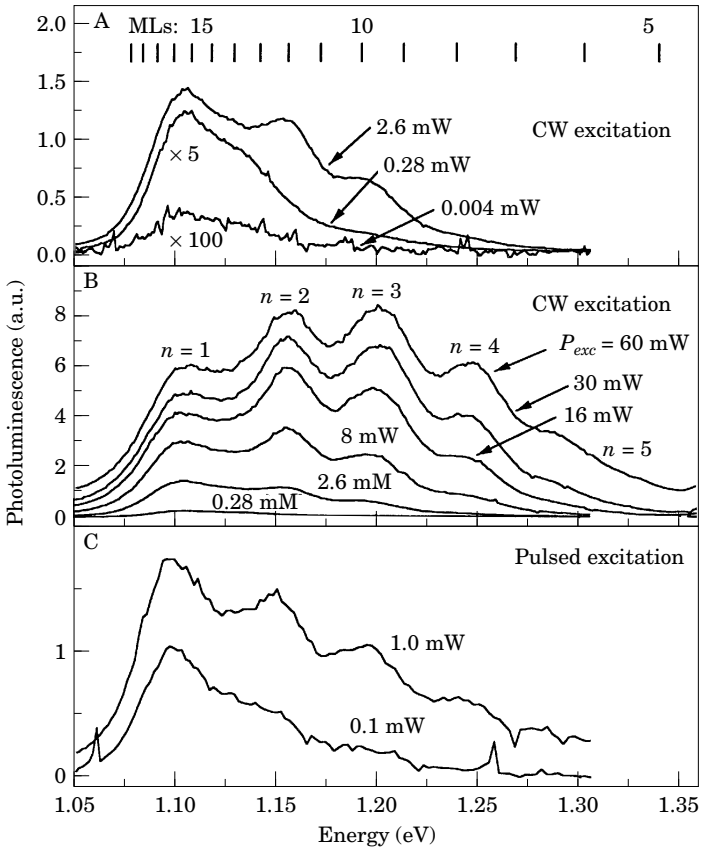

Fig. 2. Low temperature (4 K) PL spectra of $In_{0.5}Ga_{0.5}As/GaAs$ self-assembled QDs 36.5 nm in diameter displaying excited state radiative recombination as the intensity is increased. Spectra excited with a CW Ar^+ ion laser at different excitation intensities in A and B; and excited at 1.968 eV with a pulsed dye laser in C. With pulsed excitations, the excited state emission is obtained at slightly lower excitation intensities. To illustrate that the PL arises from the excited states and not from ML fluctuations in a QW, the calculated emission energies for a corresponding hypothetical QW with a various number of MLs is shown with the vertical bars at the top of figure.

4. Theoretical concepts

The expected electronic levels of the QDs were calculated with the structural information provided by the growth, TEM, and the PL results. The QD is modeled as a hemispherical cap [38], with fixed height h and radius at the base s, formed on a wetting layer of thickness t_w. The confining potential V_c is zero inside the dot and the wetting layer, and finite outside. The effective mass Hamiltonian, and adiabatic approximation are used to describe the conduction and the heavy hole valence band states in the QD. Our model includes electron-hole coulomb interaction and the influence of strain was also partially considered. The precise strain distribution in these dots is still a matter of discussion [45], so as a first approximation we have used the strain distribution typical of a QW system with the same composition, and neglected valence band mixing effects. In the adiabatic approximation, we first find the energy $E(\rho)$ corresponding to the motion along the growth direction for a given thickness of the dot at the radial coordinate ρ. The radial motion for each angular momentum channel in the effective confining potential $E(\rho)$ is next solved exactly. In order to perform these calculations, the average QD height is first estimated by computing the thickness of a QW that would emit at the same ground state energy as the QDs. The total QD thickness thus obtained is 6.0 nm. Next, from the QD

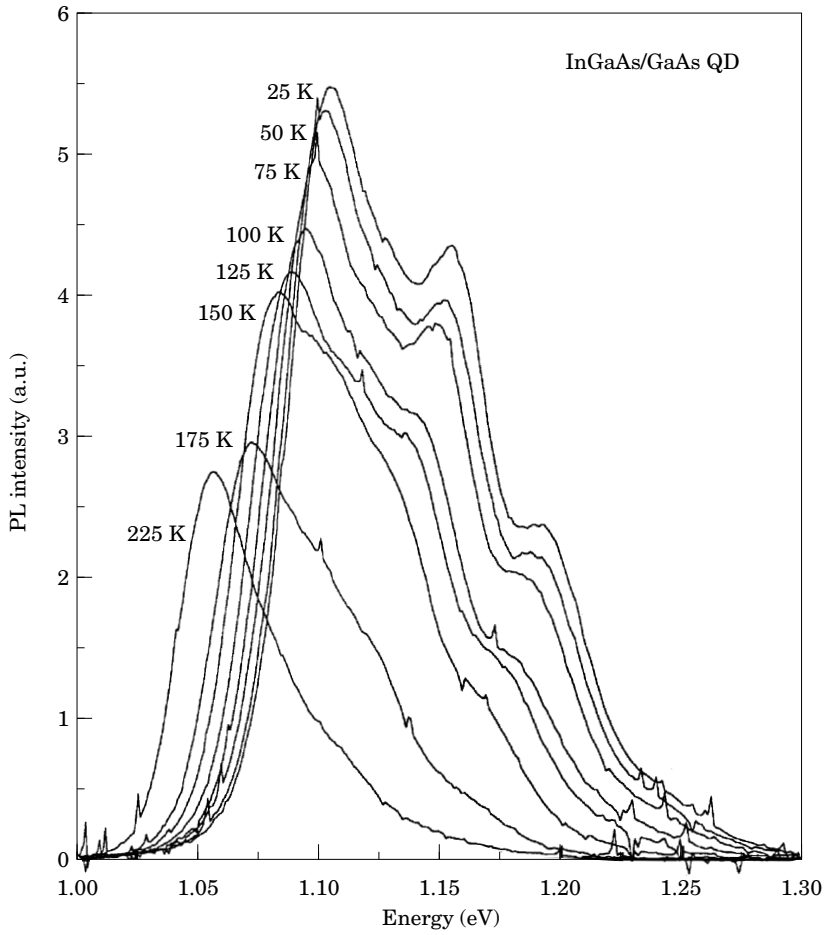

Fig. 3. Temperature dependence of the PL emission spectra of the InGaAs/GaAs dots. The optical excitation density was kept constant at ~ 50 W cm^{-2}.

coverage, average volume, and the total amount of material deposited, the WL thickness is estimated to be 1.6 nm. Results are presented in Fig. 4. The solid bars indicate the energy levels of a single QD with $s = 18$ nm, $h = 4.4$ nm, $t_w = 1.6$ nm while the dashed line shows the absorption spectrum $D(\omega)$ of an ensemble of dots, with a size distribution consistent with Fig. 1. If we are to assume the nonequilibrium distribution function $n(\omega) = e^{-\beta\omega}$, the emission spectrum of a highly excited group of QDs is given by $E(\omega) = n(\omega)D(\omega)$ as shown in Fig. 4 (solid line). It is found that there are indeed five groups of bound states below the confined states of the wetting layer. These groups correspond to states with different angular momenta m. Their grouping and spacing is consistent with a shell structure of a QD with an effective parabolic confining potential. The lineshape of the spectrum and the relative position of the peaks qualitatively corresponds to the experimental results. This simple calculation demonstrates that good agreement can be obtained between experiment and theory using an ensemble of self-assembled QDs with excited state emission. Observed discrepancies may come from differences in the real versus the assumed QD shape. The effects of exciton–exciton interactions have also been neglected. In particular, it is expected that the ground state emission is significantly broadened by bi-excitonic recombinations.

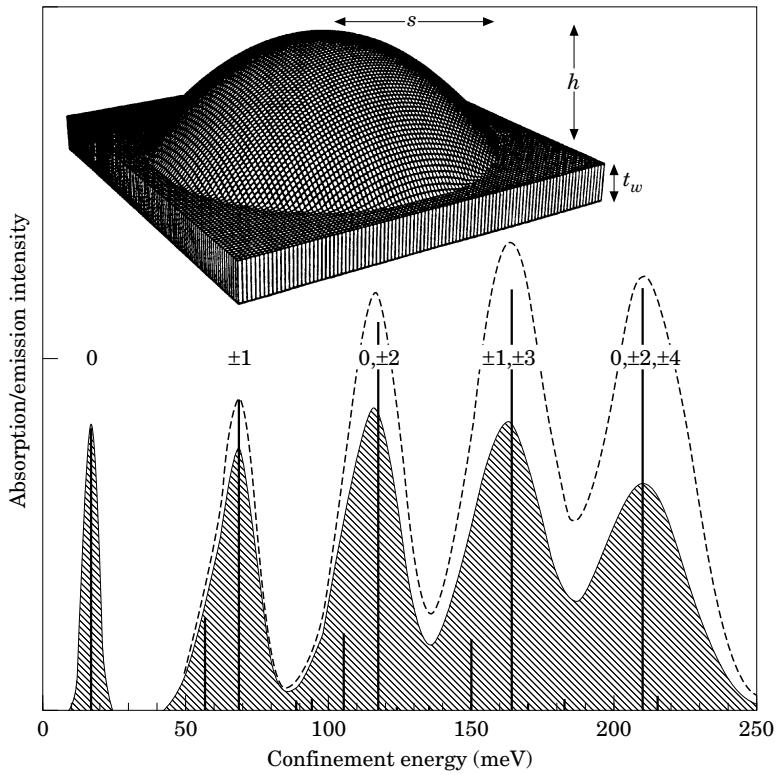

Fig. 4. Absorption spectrum (– – –) and emission spectrum (——) obtained from theoretical calculations for an ensemble containing many dots. The bars indicate the position of the energy levels for a single dot with parameter values: $s = 18$ nm, $h = 4.4$ nm and $t_w = 1.6$ nm. The amplitude of the bars is proportional to the oscillator strengths. The numbers indicate the allowed angular momenta which are consistent with the dot symmetry.

In Fig. 5 we show the energy spectrum of the $In_{0.5}Ga_{0.5}As/GaAs$ self-assembled QD with the same dimensions. In this calculation the effects of strain were approximated by calculating a uniform hydrostatic pressure shift and a uniaxial stress-induced valence band splitting. Assuming a conduction band offset of 67% the resulting electron confining potential is $V_o = 350$ meV, the effective mass of strained InGaAs $m_e = 0.067$, and the dielectric constant $\varepsilon = 12.5$. In the inset we show changes in DOS $\delta D_m(E)$ in the range of energy corresponding to the wetting layer continuum. For clarity, only a few curves, corresponding to $m = 1, 3, 6, 7$ which give the strongest resonances, have been plotted.

The average size of the dot depends on the growth conditions. The height of the potential barrier V_o in InGaAs/GaAs samples varies with In concentration. We show in Fig. 6 the dependence of the energy spectra on these parameters, i.e. the number of confined states, and the average inter-shell spacing $\omega_{e,0}$. The energy is measured from the bottom of the three-dimensional continuum in the barriers. The top frame shows the dependence of the spectrum on the size, given by the radius of the dot s-orbital for $s < 8.0$ nm one can follow the consecutive shells coming down from the wetting layer continuum as the size is increased. The inter-shell spacing decreases with increasing size and hence the almost ideally parabolic-like spectrum obtained for smaller values of s evolves into a more complicated structure of levels (the spread of higher shells comparable to inter-shell separation) for larger dots.

The bottom frame illustrates the dependence of the spectrum on the potential depth V_o at a fixed size, $s = 18$ nm and $h = 4.4$ nm. Analogously to the upper frame, we observe an increasing number of bound

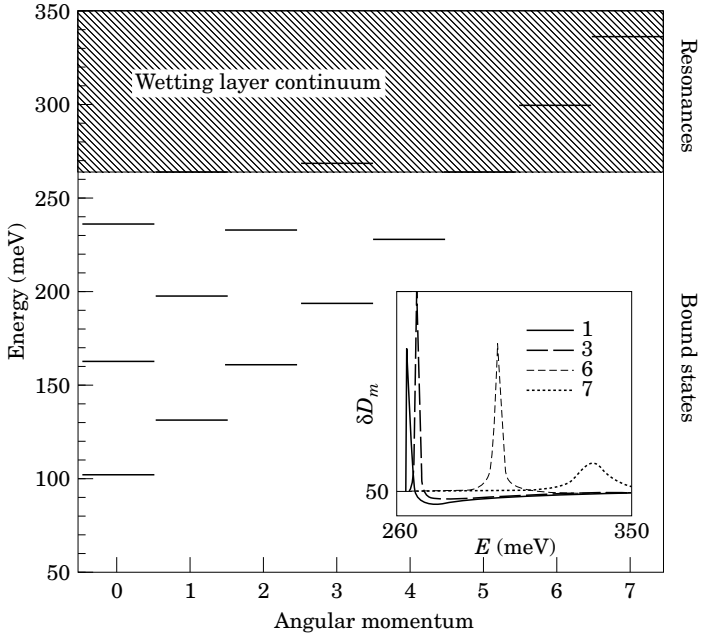

Fig. 5. The energy spectrum of bound states and wetting layer resonances in the InGaAs/GaAs dot with radius $s = 18$ nm, height $h = 4.4$ nm and depth of the confining potential $V_o = 350$ meV. The levels are degenerated due to spin and $\pm m$ symmetries. Average inter-shell spacing is $\omega_{e,0} = 30$ meV. Inset: Change in the density of states in the wetting layer continuum due to scattering potential of the dot.

states with increasing V_o. However, the inter-shell separation $\omega_{e,0}$ now grows with increasing V_o, and therefore also with increasing number of bound states. For the size of the dot chosen for this graph (corresponding to the size of the dots which can be deduced from growth, structural, and optical information, see Fig. 1), the distinct well-separated shells are obtained in the full range of V_o.

Combining the dependences shown in Fig. 6 one can design the dots systems with a desired number of confined states separated by a characteristic inter-shell excitation energy.

5. Time-resolved spectroscopy

Time-resolved spectroscopy was used to monitor the time evolution of each emission line observed, and to obtain information on the dynamics of the interband radiative recombination and the inter-sublevel thermalization. The time-dependent trace for each PL peak is shown in Fig. 7 for an average excitation intensity of 20 W cm^{-2}. The decay part of each curve was empirically fitted to a single exponential function of the form $Ae^{-t/\tau}$ in order to extract a decay time constant. The ground state as well as the first and second excited states do not seem to show a single exponential decay due to the state-filling effect, but for the dynamic range permitted by the experiment, deviations from the trial function were small. The same procedure was applied for two other excitation intensities, namely 2 W cm^{-2} and 500 W cm^{-2}. Figure 8B summarizes the results obtained. The results presented in Figs 7 and 8A and B can be summarized as follows: excited state emission and absolute saturation of the amplitude of the lower transitions are observed as the excitation intensity is increased (Fig. 8A); the decay time of a given transition increases with the excitation intensity to saturate finally slightly above 1 ns; and finally the upper transitions have faster decay times (Fig. 8B). The above observations are all consistent with state filling effects in QDs as described above.

Let us first discuss the CW PL experiment. The carriers are first created in the barrier material (GaAs),

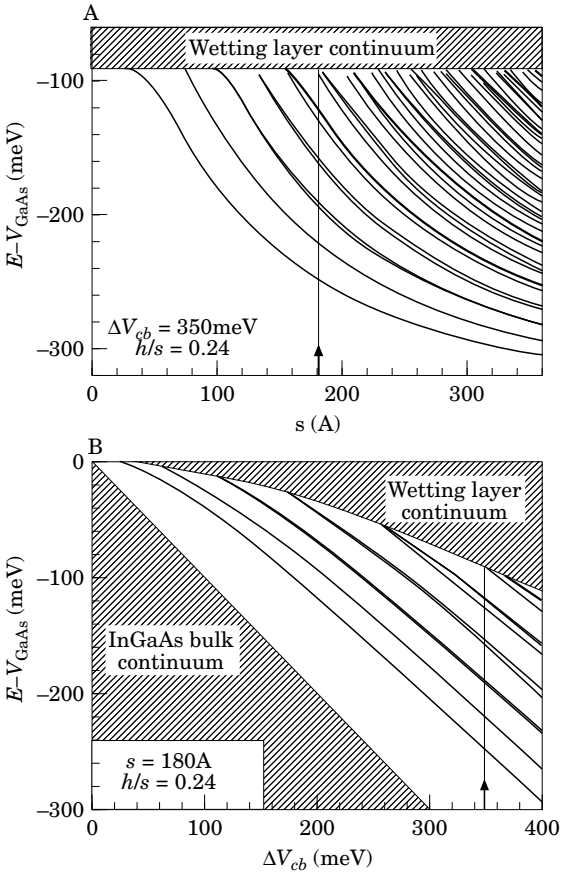

Fig. 6. Dependences of the electronic energy spectrum of the dot on size (top frame) and on the depth of confining potential V_o (bottom frame). Vertical arrows indicate the spectrum shown in Fig. 5.

and those created in the vicinity of the QD layer will be captured by the QDs. Precise information about the capture process is not available at the moment, but carriers should first fall in the 2D continuum states of the WL before being trapped by a QD. Without more precise experimental evidence, one has to consider that the carriers can then possibly fall directly into any of the available discrete bound states with no need to occupy sequentially all the excited states. However, since more states are available in higher energy levels, most carriers will enter the dot via an excited state. This implies that the inter-sublevel relaxation times are much shorter than the excited state radiative lifetimes, otherwise excited state luminescence would be observed at low excitation power (phonon bottleneck effect); not observed in Fig. 2. The carrier population and therefore the PL intensity of a given excited state will be proportional to $\tau_{isl}/(\tau_{isl}+\tau_{rad})$, where τ_{isl} is the inter-sublevel relaxation time and τ_{rad} is the radiative lifetime. This factor becomes negligible if $\tau_{isl} \ll \tau_{rad}$, and excited state PL can be observed only if τ_{isl} is comparable to τ_{rad}. Since no excited state emission is observed at low excitation intensities, the above condition must be satisfied for empty QDs, and we therefore interpret the longer decay time, before the saturation caused by the upper state feeding process, as being the radiative lifetime ($\sim$ 1 ns). However, since excited state PL can be observed at high excitation intensities, it is clear that the inter-sublevel thermalization towards the lower levels is slowed due to the reduced number of available final states caused by the state filling effect. As the inter-sublevel thermalization rate decreases and approaches

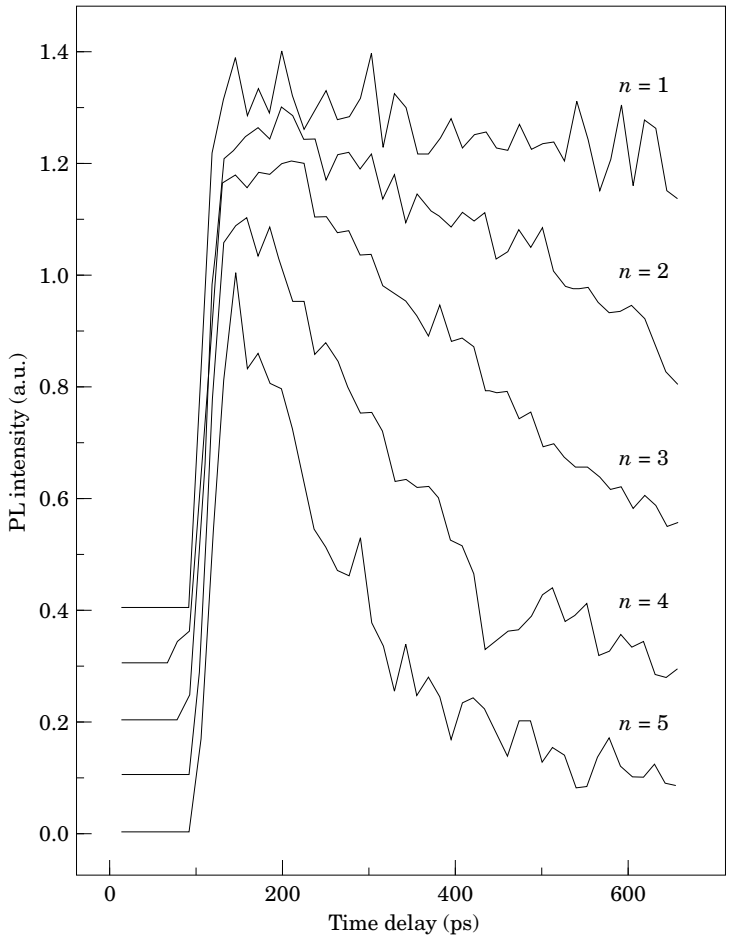

Fig. 7. Time-decay of the various emission peaks spectra obtained by up-conversion measurements. The sample was excited with a YAG pumped rhodamyne 640 dye laser system producing 5 ps pulses and emitting at 630.0 nm. The average power at the sample was 1 mW with a repetition rate of 76 MHz. Each trace was obtained at 4 K by monitoring the decay of one energy level (30 meV bandwidth for detection).

the interband radiative recombination rate for a given excited state transition, the spectra display a progressive saturation of the lower energy transitions combined with the emergence of new emission peaks originating from the upper excited states. A schematic of the carrier relaxation/capture processes is shown in Fig. 9.

For the TRPL measurements all photoexcited carriers are created within 5 ps, i.e. before any radiative recombination can occur. At this point the QDs are empty and $\tau_{isl} \ll \tau_{rad}$, therefore capture times are fast compared to the radiative lifetimes, and state filling will occur for lower average excitation powers than in the CW case. This is observed in Fig. 2. Then, after the QDs are initially filled and neglecting non-radiative recombination†, the carriers can relax either by radiative recombination or inter-sublevel relaxation, except for carriers in the ground state which can decay by radiative recombination only. When a recombination event occurs, it creates an empty state. This empty state is eventually filled by a carrier coming from the upper levels, which in turn leaves an empty state in upper levels. This cascade stops when the highest occupied

† Neglecting non-radiative recombination at 4 K is supported by the temperature dependence of the PL emission.

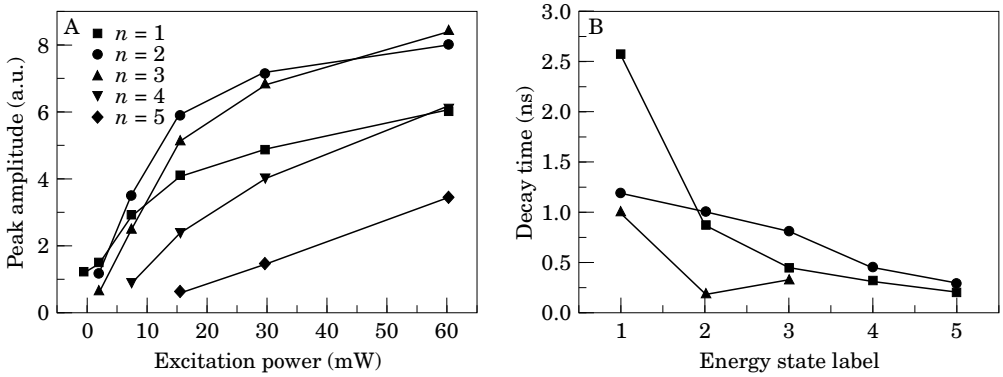

Fig. 8. Summary of the results obtained on, A, the PL peak amplitude, for $n = 1$ to $n = 5$, as a function of excitation power in the CW mode and, B, the decay time constant of the various states ($n = 1$ to $n = 5$) for three optical excitation densities, obtained in the pulsed excitation mode.

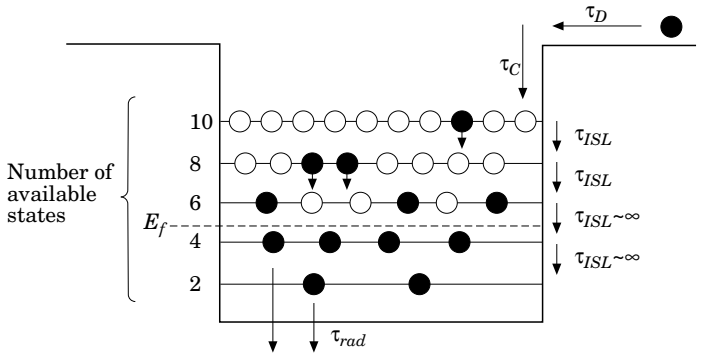

Fig. 9. Schematic of the various relaxation processes of the photogenerated carriers in the QD structure. The various symbols represent: τ_d = diffusion time, τ_c = capture time, τ_{isl} = inter-sublevel relaxation time, τ_{rad} = radiative lifetime and E_F = Fermi energy.

level loses a carrier which cannot be replaced. Thus the shorter intensity-dependent decay times of the upper excited states are a consequence of the state filling effect. Also, the non-single exponential decay of lower energy levels is caused by the constant supply of carriers coming from the upper states. For lower excitation intensity the initial occupation number $n(\omega)_0$ of all the states is lower and the number of decay channels available for excited states becomes higher, and hence the shorter decay times observed. For such case of low excitation densities, some of the excited states may be initially empty. Under these conditions, the decay time of the highest occupied level is mainly determined by the inter-sublevel relaxation time. For 2 W cm^{-2} excitation, the decay time of the $n = 3$ level is 310 ps, and for a sequential picture in which carriers can only decay to the next lowest level, this time is an estimate of the $n = 3$ to $n = 2$ inter-sublevel thermalization time. Note that since excited state luminescence can still be observed, state-filling effects are present and the empty dot inter-sublevel relaxation times are in fact much shorter than 310 ps. Inoshita and Sakaki [49] have calculated that subnanosecond inter-sublevel relaxation times can be achieved for an energy spacing of one LO phonon with a tolerance of $\sim$ 3 meV. For the sample studied in this paper, the combined electron and hole inter-sublevel spacings range from 40 to 50 meV. According to our calculations this corresponds to an electron spacing in the range of available phonons energies of 30 ± 3 meV and 36 ± 3 meV for the InAs-like and the GaAs-like LO phonon energies respectively [17, 18]. These processes might therefore contribute to

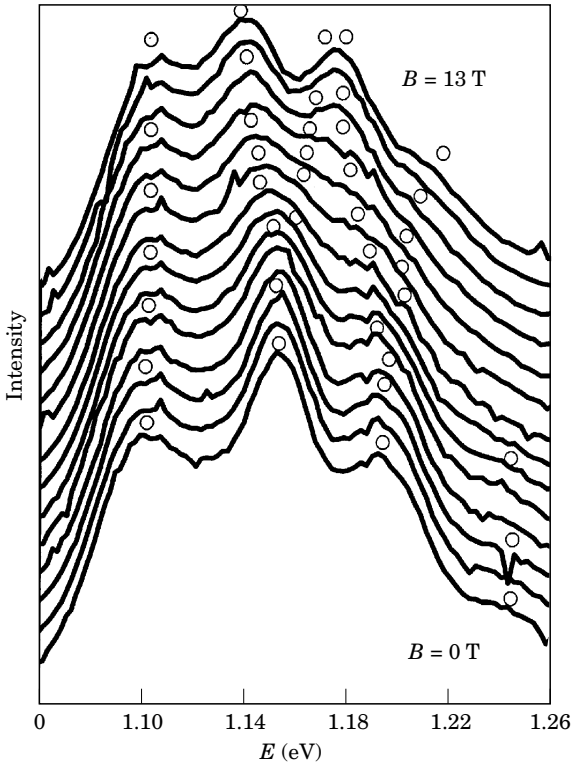

Fig. 10. The recombination spectrum of the InGaAs/GaAs quantum dots excited with 100 mW for magnetic fields $B = 0$–13 Tesla.

the fast thermalization towards the lower energy states. In addition, Auger-like processes have been suggested to explain subnanosecond carrier relaxation in small QDs [15, 21].

It is also interesting to note that the rise times for the various transitions at different excitation intensities are found to be virtually the same, and close to the temporal resolution limit of our setup, namely the 10–90% rise times are 35 ± 5 ps. For a given energy level, this time is determined by the diffusion time to the dot region (τ_d), the actual capture time from the top of the barrier to the discrete bound state considered (τ_c) and the inter-sublevel dynamics. If the rise time was dominated by the capture time (i.e. slow τ_c), one would expect τ_{rise} to be different for each level since Fig. 2 indicates that the lower levels will be filled first. Moreover, in this case the inter-sublevel dynamics would play a role and depending if a particular level is beneath or above the initial quasi-Fermi level its rise time should change dramatically. Thus for slow τ_c one expects the rise times to be a function of energy level and excitation density. Equal rise times for all states at all intensities suggests that τ_{rise} is rather limited by carrier diffusion, which would imply that the actual capture times (τ_c) are much shorter than 35 ps. Future femtosecond resonant excitation experiments would help to clarify this fast capture dynamics.

6. Magneto-photoluminescene

The evolution of the recombination spectrum of the highly excited dot with the magnetic field is shown in Fig. 10. At $B = 0$ T, the spectrum consists of three well-resolved peaks at 1.102, 1.155, 1.197 eV and a fourth weak structure at 1.245 eV. With increasing magnetic field the spectrum does not change significantly

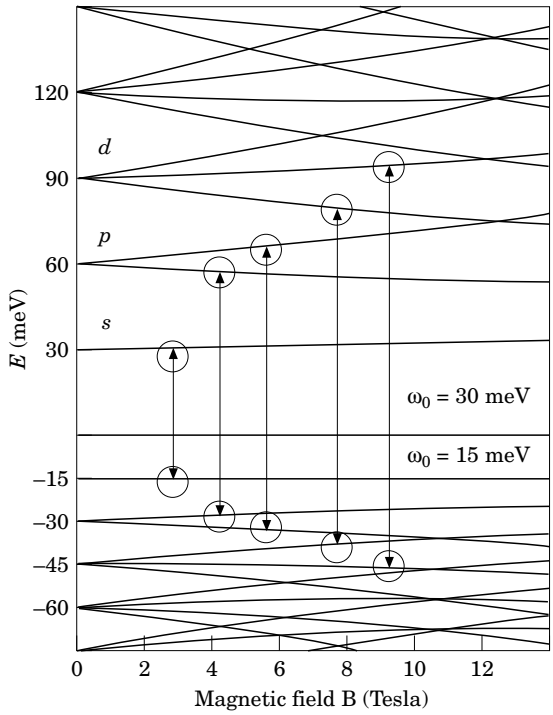

Fig. 11. The energy spectrum of electrons and holes as a function of the magnetic field. Optical transitions between s, p, d, ... electron and hole states are indicated by the arrows.

until $B = 7$ T, where the spectrum broadens in the spectral range 1.15–1.20 eV. The broadening decreases and sharp spectral features are recovered by $B = 12$ T. This broadening can be interpreted by the splitting of the second and third peaks, as indicated by the circles. A Gaussian fitting gave the evolution of peaks with the magnetic field.

The full theoretical treatment of the effect of the magnetic field on the transition energy of the various excited states and ground state inside the dot can be found elsewhere [31, 50, 51]. Here, we will provide only a short summary of those results.

As discussed in Section 4, both electrons and holes inside the QDs are confined by an effective parabolic potential. With the magnetic field B applied normal to the plane of the dot, the single particle spectra consist of Fock–Darwin (FD) levels. The FD energies, eigenstates and angular momenta are those of two harmonic oscillators, whose frequencies are equal at $B = 0$ and are tuned by the magnetic field [52]. In the absence of a magnetic field, the degenerate shells can be labeled as s, p, d, ... with degeneracies 2, 4, 6, ... including spin. The magnetic field evolution of the single particle energy spectrum of electrons and holes is shown in Fig. 11. The optically allowed transitions, indicated with arrows, indicate the recombination spectrum of $N = 10$ non-interacting electrons and holes. The $B = 0$ T spectrum consists of three peaks corresponding to three shells. The degeneracies of the shells are removed by the increasing magnetic field and transitions originating from the p and d shells split. In the $B = 11$–12 T range the level crossing leads to the restoration of the shell structure and some of the transitions become degenerate. Therefore, on the basis of the non-interacting energy spectrum one expects to see sharp peaks in the recombination spectrum at $B = 0$ T, followed by the broadening due to splitting and level crossing, and followed again by sharp peaks in the $B = 11$–12 T due to the formation of the second shell. The effect of carrier–carrier interaction in this simplified picture has been

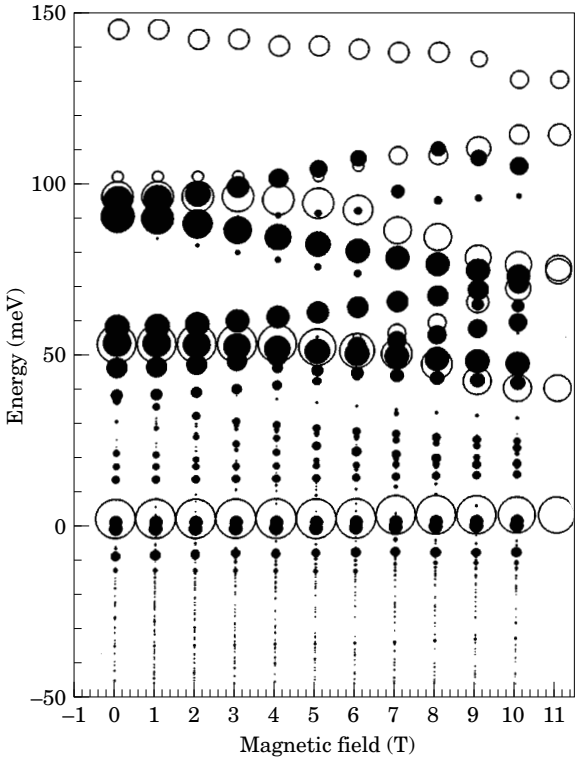

Fig. 12. Measured (○) and calculated (●) recombination spectrum from dots filled with an average of $N = 5$ excitons.

fully addressed elsewhere [51]. The splitting and subsequent restoration of the emission lines is therefore a specific characteristic of the 0D excited states.

Our analysis of experimental results follows the work on electron–hole systems in strong magnetic fields by Potemski *et al*. [53]. With increasing excitation power, excitons diffuse, relax and accumulate in QDs. In steady state, in an ensemble of QDs, the number of excitons fluctuates around a mean value $\langle N \rangle$. The experimentally observed spectrum $E(\omega)$ is therefore averaged over a spectrum of dots with N excitons with probability $P(N)$; i.e. $E(\omega) = \sum_N P(N)E(N, \omega)$. Assuming a Gaussian distribution $P \sim \exp(-(N - \langle N \rangle)^2/\Delta^2)$ with $\langle N \rangle = 5$ and $\Delta = 5$, a calculated recombination spectrum is compared with experiment in Fig. 12. The full dots correspond to the calculated and empty dots to the measured spectrum. An overall agreement and level spacing between the calculated and the measured spectrum is very good. The calculation predicts a broadening and level splitting in the 5–10 T range for the two higher peaks, in good agreement with the experiment.

7. Conclusion

In conclusion, excited state PL was obtained in $In_{0.5}Ga_{0.5}As/GaAs$ self-assembled QDs, and up to five QD bound states were observed. Up-conversion has been used to measure the decay time of the excited state emission. The fast inter-sublevel thermalization of the bare excited states which leads to a progressive state-filling of the lower-energy states allowed the quasi-Fermi level to be raised by more than 200 meV due to the combined large inter-sublevel spacing and the low density of states. The decay time of each transition obtained under various excitation conditions has been used to evaluate the excited state radiative lifetime which is estimated to $\sim$ 1 ns (similar to the ground state lifetime), and the bare inter-sublevel thermalization time

which is estimated to a few hundred ps. Finally, we have measured the recombination spectrum of strongly correlated electrons and holes in 0D in a magnetic field. The structures in the recombination spectrum from a droplet of many excitons reflects the 0D quantized density of single particle states.

Acknowledgements—Part of this research was supported by NSF Science and Technology Center QUEST (DMR #91-20007), and by an AFOSR grant (#F49620-92-J-0124). One of us (S.R.) would also like to acknowledge NSERC for their additional support.

References

[1] Kerry J. Vahala, IEEE J. Quantum Electronics **24**, 523 (1988).
[2] E. Kapon, Proc. IEEE **80**, 398 (1992).
[3] H. Temkin, G. J. Dolan, M. B. Panish, and S. N. G. Chu, Appl. Phys. Lett. **50**, 413 (1987).
[4] K. Brunner, U. Bockelmann, G. Abstreiter, M. Walther, G. Böhm, G. Tränkle, and G. Weimann, Phys. Rev. Lett. **69**, 3216 (1992).
[5] Y. Hirayama, Y. Suzuki, S. Tarucha, and H. Okamoto, Jpn. J. Appl. Phys. **24**, L516 (1985).
[6] K. Kash, J. M. Worlock, M. D. Sturge, P. Grabbe, J. P. Harbison, A. Scherer, and P. S. D. Lin, Appl. Phys. Lett. **53**, 782 (1988).
[7] I.-H. Tan, R. Mirin, V. Jayaraman, S. Shi, E. Hu, and J. Bowers, Appl. Phys. Lett. **61**, 300 (1992).
[8] K. Kash and J. Lumin. **46**, 69 (1990).
[9] D. J. Eaglesham and M. Cerullo, Phys. Rev. Lett. **64**, 1943 (1990).
[10] S. Z. Chang, T. C. Chan, and S. C. Lee, J. Appl. Phys. **73**, 4916 (1993).
[11] C. W. Snyder, J. F. Mansfield, and B. G. Orr, Phys. Rev. **B 46**, 9551 (1992).
[12] L. Goldstein, F. Glas, J. Y. Marzin, M. N. Charasse, and G. Le Roux, Appl. Phys. Lett. **47**, 1099 (1985).
[13] J. Y. Marzin, J. M. Gerard, P. Voisin, and J. A. Brum, in *Semiconductor and Semi-Metals*, edited by T. P. Pearsall, Vol. 32, Academic Press, New York, N. Y.: p.55 (1990).
[14] Q. Xie, P. Chen, and A. Madhukar, Appl. Phys. Lett. **65**, 2051 (1994).
[15] H. Benisty, C. M. Sotomayor-Torrès, and C. Weisbuch, Phys. Rev. **B 44**, 10945 (1991); H. Bensity, Phys. Rev. **B 51**, 13281 (1995).
[16] U. Bockelmann and G. Bastard, Phys. Rev. **B 42**, 8947 (1990); U. Bockelmann and T. Egeler, Phys. Rev. **B 46**, 15574 (1992); U. Bockelmann, Phys. Rev. **B 48**, 17637 (1993).
[17] S. Fafard, R. Leon, D. Leonard, J. L. Merz, and P. M. Petroff, Phys. Rev. **B 52**, 5752 (1995).
[18] R. Heitz, M. Grundmann, N. N. Ledentsov, L. Eckey, M. Veit, D. Bimberg, V. M. Ustinov, A. Y. Egorov, A. E. Zhukov, P. S. Kop'ev, and Z. I. Alferov, Appl. Phys. Lett. **68**, 361, (1996).
[19] B. Benett, B. V. Shanabrook, and R. Magno, Appl. Phys. Lett. **68**, 958 (1996).
[20] S. Raymond, S. Fafard, S. Charbonneau, R. Leon, D. Leonard, P. M. Petroff, and J. L. Merz, Phys. Rev. **B 52**, 17238 (1995).
[21] Al. L. Efros, V. A. Kharchenko, and M. Rosen, Solid State Commun. **93**, 281 (1995).
[22] D. Leonard, S. Fafard, K. Pond, Y. H. Zhang, J. L. Merz, and P. M. Petroff, J. Vac. Sci. Technol. **B 12**, 2516 (1994).
[23] S. Fafard, R. Leon, D. Leonard, J. L. Merz, and P. M. Petroff, Phys. Rev. **B 50**, 8086 (1994).
[24] J.-Y. Marzin, J.-M. Gérard, A. Izraël, D. Barrier, and G. Bastard, Phys. Rev. Lett. **73**, 716 (1994).
[25] S. Fafard, D. Leonard, J. L. Merz, and P. M. Petroff, Appl. Phys. Lett. **65**, 1388 (1994).
[26] M. Grundmann, J. Christen, N. N. Ledentsov *et al*., Phys. Rev. Lett. **74**, 4043 (1995).
[27] R. Nötzel, J. Temmo, A. Kozen, T. Tamamura, T. Fukui, and H. Hasegawa, Appl. Phys. Lett. **66**, 2525 (1995).
[28] J. M. Moison, F. Houzay, F. Barthe, L. Leprince, E. André, and O. Vatel, Appl. Phys. Lett. **64**, 196 (1994).
[29] G. Wang, S. Fafard, D. Leonard, J. E. Bowers, J. L. Merz, and P. M. Petroff, Appl. Phys. Lett. **64**, 2815 (1994).

[30] S. Fafard, Z. Wasilewski, J. McCaffrey, S. Raymond, and S. Charbonneau, Appl. Phys. Lett. **68**, 991 (1996).
[31] A. Wojs, P. Hawrylak, S. Fafard, and L. Jacak, Phys. Rev. **B**, to be published.
[32] M. Grundmann, N. N. Ledentsov, O. Stier, D. Bimberg, V. M. Ustinov, P. S. Kop'ev, and Z. I. Alferov, Appl. Phys. Lett. **68**, 979, (1996).
[33] H. Lipsanen, M. Sopanen, and J. Ahopelto, Phys. Rev. **B 51**, 13868 (1995).
[34] A. Zrenner, L. V. Butov, M. Hagan, G. Abstreiter, G. Böhm, and G. Weimann, Phys. Rev. Lett. **72**, 3382 (1994).
[35] D. Gammon, E. S. Snow, and D. S. Katzer, Appl. Phys. Lett. **67**, 2391 (1995).
[36] K. Brunner, G. Abstreiter, G. Böhm, G. Tränkle, and G. Weimann, Phys. Rev. Lett. **73**, 1138 (1994).
[37] Q. Xie, A. Madhukar, P. Chen, and N. P. Kobayashi, Phys. Rev. Lett. **75**, 2542 (1995).
[38] D. Leonard, K. Pond, and P. M. Petroff, Phys. Rev. **B 50** 11687 (1994).
[39] M. V. Marquezini, M. J. S. P. Brasil, J. A. Brum, P. Poole, S. Charbonneau, and M. C. Tamargo, Surface Science, EP2DS-XI conference proceedings, Surface Science **361/362**, 810 (1996).
[40] H. Drexler, D. Leonard, W. Hansen, J. P. Kottaus, and P. M. Petroff, Phys. Rev. Lett **73**, 2252 (1994).
[41] P. D. Wang J. L. Merz, S. Fafard, R. Leon, D. Leonard, G. Medeiros-Ribeiro, M. Oestreich, P. M. Petroff, K. Uchida, N. Miura, H. Ariyama, and H. Sakaki, accepted in Phys. Rev. **B 53**, 16458 (1996).
[42] S. Raymond, P. Hawrylak, C. Gould, P. Zawadzki, A. Sachrajda, S. Charbonneau, S. Fafard, D. Leonard, P. M. Petroff, and J. L. Merz, to be published.
[43] D. Gammon, E. S. Snow, and D. S. Katzer, Surface Science, EP2DS-XI conference proceedings to be published in Surface Science.
[44] S. Fafard, S. Raymond, G. Wang, R. Leon, D. Leonard, S. Charbonneau, J. L. Merz, P. M. Petroff, and J. E. Bowers, Surface Science, EP2DS-XI conference proceedings, Surface Science, **361/362** 778 (1996).
[45] M. Grundmann, O. Stier, and D. Bimberg, Phys. Rev. **B 52**, 11969 (1995).
[46] R. Steffen, T. Koch, J. Oshinowo, F. Faller, and A. Forchel, Surface Science, EP2DS-XI conference proceedings to be published in Surface Science.
[47] J. Shah, IEEE J. Quantum electron. **QE-24**, 276 (1988).
[48] The PL spectra obtained in various regions of a 1.5×2 mm sample displayed no significant spectroscopic variations, indicating that this small piece contains no significant macroscopic inhomogeneities. This sample was cut in two parts which were then dedicated to the TEM and the optical studies presented here.
[49] T. Inoshita and H. Sakaki, Phys. Rev. **B 46**, 7260 (1992).
[50] A. Wojs and P. Hawrylak, Phys. Rev. **B 51**, 10880 (1995).
[51] S. Raymond, P. Hawrylak, C. Gould, A. Sachrajda, S. Fafard, M. Potemski, S. Charbonneau, D. Leonard, P. M. Petroff, and J. L. Merz, submitted to Phys. Rev. Lett. (1996).
[52] P. Hawrylak, Phys. Rev. Lett. **71**, 3347 (1993).
[53] M. Potemski, *Proceedings of the International Conference on High Magnetic Fields in Semiconductors*, edited by D. Heimann, (1996).